Transposing an active fault database into a fault-based seismic hazard assessment for Nuclear facilities.
Part B: Impact of fault parameter uncertainties on a site-specific PSHA exercise in the Upper Rhine Graben, Eastern France

5 Thomas Chartier[1,2], Oona Scotti[1], Christophe Clément[1], Hervé Jomard[1],Stéphane Baize[1]

[1]Bureau d'Evaluation des Risques Sismiques pour la Sûreté des Installations, Fontenay-aux-Roses, 92262, France
[2]Today at Département de Géosciences, Ecole Normale Supérieure, Paris, 75005, France

10 *Correspondence to*: Thomas Chartier (chartier@geologie.ens.fr)

Abstract. We perform a fault-based PSHA exercise in the Upper Rhine Graben to quantify the relative influence of fault parameters on the hazard at the Fessenheim Nuclear Power Plant site. Specifically, we show that the potentially active faults described in Part A of this paper (Jomard et al., submitted this issue) are the dominant factor in hazard estimates at the low annual probability of exceedance relevant for the safety assessment of nuclear installations. Geological information
15 documenting the activity of the faults in this region, however, remains sparse, controversial and affected by a high degree of uncertainty. A logic tree approach is thus implemented to explore the epistemic uncertainty and quantify its impact on the seismic hazard estimates. Disaggregation of the Peak Ground Acceleration (PGA) hazard at 10,000 years return period shows that the Rhine River Fault is the main seismic source controlling the hazard level at the site. The choice of Ground Motion Prediction Equations (GMPE) is the major source of uncertainty. Nonetheless the parameters describing the
20 geometry and the seismic activity of the faults (dip, width, slip rate) also have an impact on the result depending on the GMPE used. The uncertainty on the slip rate of the Rhine River Fault is the second most dominant factor controlling the uncertainty on the seismic hazard level. Uncertainty on slip rate estimates from 0.04 mm/yr to 0.1 mm/yr results in up to 40% increase in hazard levels at the 10,000 years return period target depending on the GMPE used and the spectral frequency of interest. Reducing epistemic uncertainty in future fault-based PSHA studies at this site will thus require (1)
25 performing in-depth field studies to better characterize the seismic potential of the Rhine River Fault; (2) complementing GMPEs with more physics-based modeling approaches to better account for the near-field effects of ground motion and (3) improving the modeling of the background seismicity. Indeed, in this exercise, we assume that background earthquakes can only host M< 6.0 earthquakes. However, this assumption is debatable, since faults that can host M>6.0 earthquakes have been recently identified at depth within the Upper Rhine Graben (see Part A) but are not accounted for in this exercise since
30 their potential activity has not yet been described.

1 Introduction

The Upper Rhine Graben (URG) is one of the most seismically active areas in metropolitan France, where active faulting along north-south structures has been documented in the literature [see part A - (Jomard et al., submitted this issue) and references therein]. The close proximity of a nuclear site to these faults, potential sources of M>6.0 earthquakes, requires

5   setting up fault models based on the available geological information and developing tools to compute the seismic hazard posed by these faults in a probabilistic framework. The geological evidences of their activity and corresponding fault model are discussed in the companion paper (Part A). The purpose of this paper is to show the shortcomings and challenges posed by the modelling of faults in probabilistic seismic hazard calculations.

Probabilistic seismic hazard assessment (PSHA) is a method classically used to assess seismic hazard for a single site or for

10   a group of sites hence creating a seismic hazard map. The first step of PSHA following a Cornell-McGuire (Cornell 1968; McGuire 1976) approach is the characterization of the seismic sources, including seismogenic zones and active faults. The parameters of the slow moving faults of the URG, with slip rates less than 0.1 mm/yr, are affected by large uncertainties because their recent activity isn't necessarily well expressed in the landscape. In this study, we explore the range of associated uncertainties by setting up a logic tree exploring the fault parameters and uncertainties as described in the faults

15   data base (BDFA - see part A). For critical facilities, the PSHA needs to be calculated for low probabilities of exceedance (long return periods) of the ground motion (cf. International Atomic Energy Agency, IAEA 2010). We focus the discussion on the 10,000 years return period ground motion hazard computed with the CRISIS2014 software (Ordaz et al 2014).

2 A fault model in a Probabilistic Seismic Hazard Assessment (PSHA)

2.1 Defining the geometry of fault sources and the background source

20   Two types of sources need to be defined in a fault-based PSHA model approach: background sources and fault sources. Both types of sources can generate earthquakes over a wide spectrum of magnitudes. In this study we implement a very simplistic approach by allowing higher magnitude events (M>=6.0) to occur only on faults. The delicate issue of how to properly partition earthquakes between background and fault sources is not the scope of this study and should be tackled in the future development of hazard model for the area.

25   The background zone was defined using the zoning scheme of Baize et al 2013 and a homogenous Mw catalogue derived from the " Laboratoire de détection géophysique" (CEA/LDG, 2011) catalog for the instrumental part, and FPEC (the IRSN contribution to SHEEC, Stucchi et al 2013) for the historical part.

Following the BDFA (Figure 4 of Part A, Annex), three fault systems are present in the site vicinity: the West Rhenish Fault system limiting the URG to the west, the Rhine River Fault system lying within the graben and the Black Forest Fault system

30   limiting the URG to the east. These faults are considered to be strictly normal faults in this hazard model. In this southernmost part of the URG, BDFA points out three individualized segments for each considered fault system. In this

study only single segment fault ruptures are considered; multiple fault rupture scenarios should be considered in a later study. The maximum possible magnitude that each fault segment can release is then determined based on the mean value given by the Wells and Coppersmith (1994) empirical scaling relationship, hereafter WC94, and using the surface area of each fault segment. Geophysical information allows us to constrain the 3D geometry of the faults, with some uncertainty

5 about the dip, and the seismogenic depth (between 15 and 20 km according to the microseismicity presented by Edel et al, 2006). The slip rates of each segment are also highly uncertain, as presented in the companion paper (Part A). In order to explore the impact of these uncertainties in the seismic hazard calculations different geometrical hypothesis and published slip rates are considered as shown in Table 1.

2.2 Modelling seismicity on faults

10 In order to compute seismic hazard related to faults it is necessary to transform their slip rates into an annual number of earthquakes per magnitude bin. In this study we consider that all the slip rate is converted into seismic moment rate. The classical approach to convert slip rate into seismic moment rate is based on the following relationship Eq. (1):

$$\dot{M}_0 = \mu A V \dot{s} \tag{1}$$

Where $\dot{M}_0$ is the seismic moment rate (10^{-5} N.m.yrs^{-1}), μ is the shear modulus (10^{-5}N.m^{-2}), A is the surface rupture area (m^2)

15 and $\dot{s}$ is the slip rate (m.yrs^{-1}). Then relating moment magnitude and seismic moment (in N.m) through the Hanks and Kanamori (1979) relationship Eq. (2):

$$M_0 = 10^{(1.5\,M+9.1)} \tag{2}$$

Finally, it is necessary to make hypothesis about how this moment rate is released. In this study we considered only two hypotheses of Magnitude Frequency Distribution (MFD):

20   -seismic moment rate of faults is released by ruptures that involve the entire surface area of the fault and thus producing events of the same characteristic magnitude (Wesnousky, 1986) equal to the maximum magnitude defined in Table 1.

       -seismic moment rate of faults is released by different magnitudes following the Gutenberg-Richter (1954) (GR) hypothesis which states that the expected number of earthquakes in a given region and time span, will be:

25 $$N(m \geq M) = 10^{(a-b\,M)}, \tag{3}$$

where M is the earthquake magnitude, a and b are constants, and N is the expected number of earthquake with a magnitude m greater than M.

In the characteristic earthquake hypothesis, the annual rate of the event $\lambda\,(M = M_{characteristic})$ is deduced from the

30 following equation:

$$\lambda\,(M = M_{characteristic}) = \frac{\dot{M}_0}{M_0} \tag{4}$$

In the GR hypothesis, the MFD is defined between a value Mmin below which earthquakes are considered as non-damaging and a value Mmax which is the maximum magnitude possible on the fault. The rate of events of magnitudes greater than the magnitude of interest $\lambda(M \geq M_{min})$ is deduced from the following equation:

$$\lambda(M \geq M_{min}) = \frac{1.5 - b}{b} \times \frac{1 - 10^{-b(M_{max} - M_{min})}}{10^{-b(M_{max} - M_{min})} \times (10^{1.5 \times M_{max} + 16.05} - 10^{1.5 \times M_{min} + 16.05})} \times \mu \times A \times V \qquad (5)$$

5   In this study, the slope of the GR distribution is assumed equal to 1 (b value = 1) and the shear modulus is fixed at 3.10^{10} N.m^{-2} as a standard value. Table 2 summarizes the seismic activity of each fault considered in this exercise deduced from published slip rates and assuming either a characteristic or a GR earthquake magnitude distribution.

3 Logic tree explored in this study

The classical way to explore epistemic uncertainties in seismic hazard assessment is to set up a logic tree (LT).

10   In this study we explore the following epistemic uncertainties (Figure 1):

1.   The localization of the deformation in the Rhine Graben. Two geodynamical hypotheses are proposed in the literature: one in which deformation is accommodated essentially on the Rhine River and the West Rhenish faults and an alternative one which considers that deformation is more localized on the Black Forest and the West Rhenish faults. However, most of the authors consider that the deformation today occurs mainly within the URG and much

15   less along the flanks of the graben (Schumacher, 2002; Rotstein & Schaming, 2011). Therefore, the branch where the deformation is accommodated along the Rhine River fault is weighted stronger in the logic tree (0.8).

2.   The seismogenic depth, (impacting the width of the faults). Two seismogenic depths are considered of 15 and 20 km with equal weights based on both the recorded instrumental seismicity (Edel et al., 2006) and the interpretation of a crustal scale seismic profile (DEKORP-ECORS, Brun et al. 1992).

20   3.   The geometries of faults at depth: We explore two values of the faults dip angle with the same weight.

4.   The distribution of seismicity on faults: characteristic and GR earthquake magnitude distributions are attributed the same weight in the logic tree. There is no information in the region that could be used to justify the use of one approach rather than the other.

5.   Slip rate: equal weights are attributed to the lower and higher slip rate values assessed from the vertical

25   displacements of the geological markers described in Niviere et al. 2008 (see Part A).

6.   Ground Motion Prediction Equations (GMPE): four equations widely used in PSHA applications are considered in the exercise (Table 3). These equations are valid for the range of magnitude and distance relevant for our study and representative of several ground motion datasets. These equation use different distance metrics: the shortest distance to the rupture R_{Rup}, the shortest distance to the projection of the rupture at the surface R_{JB}, and the distance to the

30   hypocenter R_{Focal}. The Vs30 parameter (mean shear wave velocity in the upper 30 m of the soil column) is set at 600 m.s^{-1} to represent the sedimentary conditions of the URG.

4 Results

Figure 2a presents the weighted mean Uniform Hazard Spectra (UHS) at 10,000 years return period for each GMPE resulting from the exploration of the logic tree (Figure 1).The UHS hazard level strongly depends on the GMPE used. Each GMPE shows very different dispersion of the results around their weighted means as shown for the Peak Ground

5   Acceleration (PGA) in Figure 2b. PGA dispersions differ from one GMPE to the other due to their different sensitivities to the parameters explored, in particular the geometry of the faults.

In order to visualize the results, let us consider a singlebranch of the logic tree: Rhine River Fault and the West Rhenish faults active, seismogenic depth of 15 km, steepest dip of the faults, slowest slip rate, Gutenberg-Richter frequency-magnitude distribution and CB08 (Figure 2a, dotted line). As Figure 3 shows, a fault-based PSHA at 10,000 years return

10   periods leads to a higher level of hazard for sites located in close vicinity of the most active faults. In order to further highlight the faults' contribution let us compare disaggregation of hazard for this branch at 475 and 10,000 years return period for PGA (0.06 g and 0.27 g, respectively). Figure 4a shows that at 475 years return period more than 70 % of the hazard is controlled by events in the 5 - 5.5 magnitude range located at less than 40 km from the site. Hazard levels are thus entirely controlled by the activity rates modeled in the background derived from the earthquake catalogue. In this case, the

15   way in which the background region is modeled becomes paramount. On the other hand at 10,000 years return period, which is the focus of this paper, hazard levels at the site, is predominantly controlled by the larger magnitude events modeled on the faults. In this case, the main fault contributing to the hazard is the Rhine River fault, which is 7 km distant from the site of interest, with magnitude 6 or greater events occurring roughly every 10,000 years (Table 2). Note however, that even at this target probability level, earthquakes modeled in the background region still contribute up to 30 % (Figure 4b) of the

20   hazard at the site of interest.

5 Sensitivity study

In order to quantify the impact of each epistemic uncertainty explored we perform a sensitivity study using the same branch of the logic tree: Rhine River Fault and the West Rhenish faults active, seismogenic depth of 15 km, steepest dip of the faults, slowest slip rate, Gutenberg-Richter frequency-magnitude distribution.

25

SHAPE OF THE MFD (Figure 5a)

The characteristic earthquake MFD leads to systematically higher spectral acceleration compared to GR MFD for this target probability level and the site of interest, with however a small impact (<10 %) on the dispersion of the results (Figure 5a).

30   GEOMETRY AT DEPTH (Figure 5b, c)

An increase in seismogenic depth and a reduction of the fault dip both lead to an increase of fault surface area hence an increase of the earthquake rates modelled on the faults (see Equation 5). Figure 5b shows that the increase in seismogenic

depth has a small effect on the UHS calculated using the GMPEs BA08, CB08 and Zh06 and no effect when using the GMPE CF08. The latter GMPE uses a R_{Focal} metric thus the effect of increase of the earthquake rate on the hazard is balanced by the increase of the R_{Focal} distances since earthquakes are generated deeper.

The reduction of the fault dip leads to a 10 to 15% increase of the UHS. Given the position of the site compared to the Rhine River Fault (Figure 3), the source-to-site distance is reduced for all metrics and the earthquake rate increase. Both effects induce a higher UHS at the site of interest.

DEFORMATION MODEL (Figure 6)

Figure 6 shows that hazard levels at the site of interest are around 15 % higher when the activity is considered on the Rhine River fault compared to the branch where the activity is on the Black Forest Fault. In spite of its lower maximum magnitude and slip rate, the Rhine River fault is located closer to the site of interest and thus induces higher hazard at the site.

SLIP RATE (Figure 7)

Uncertainty in the slip rate estimates of faults on the other hand, which in moderate seismicity regions is often high, leads to considerable dispersion of the resulting hazard levels. For the case of the Rhine River Fault for example, an increase in slip rate from 0.04 mm/yr to 0.1 mm/yr results in a 2.5 fold increase in seismic productivity and a roughly 40% increase in hazard levels (Figure 7) depending on the GMPE. Thus reducing epistemic uncertainty on the slip rate of faults is as important as reducing epistemic uncertainties in GMPE when fault-based PSHA is performed at this site.

6 Conclusion

The exercise conducted in this paper shows that the seismic hazard at 10,000 years return period for the Fessenheim Nuclear power plant site is mainly controlled by the activity of the Rhine River and Black Forest faults.. Since our site of study is very close to the Rhine River fault, the result of the hazard calculation is highly dependent on the input parameters characterizing the seismic potential of this fault. This study highlights the slip-rate attributed to the Rhine River fault and the choice of GMPE as the main sources of the variability of the seismic hazard. The uncertainty on the slip rate of the Rhine-River fault leads to a 40% variability of the hazard at 10,000 years while uncertainties in the shape of the MFD and the geometry at depth induce a 10 to 15 % variability of the hazard. This study has clearly pointed out the need to better constrain the slip rates of faults and to choose GMPEs that are as much as possible based on data recorded in close proximity to faults in order to better constrain the hazard assessment at the site.

7 Perspectives

The fault-based PSHA will need to evolve towards more realistic rupture scenarios. The 2016 earthquakes (M7.8 Kaikoura multiple segment rupture in New Zealand, M6-6.5 sequence in Central Italy and M6.5-7 Kumamoto triplet in Japan) remind

us that the representation of faults in our models is still too simplistic. Complex rupture scenarios have occurred and should be properly accounted for in more realistic fault-based approaches. Moreover, future hazard models should aim to taking into account the complexity of the regional deformation and assess the part of strike-slip deformation suggested by some focal mechanisms and not considered in this study.

5   In the present paper, the background seismicity was implemented in a very basic manner. We have limited the maximum magnitude that can occur in the background at 6.0. However, we stress that blind faults, capable of generating M> 6.0 known to be present at depth (part A of this paper) will somehow need to be accounted for..

A study is presently ongoing in the Upper Rhine Graben to better constrain the recent activity of the fault system (Baize et al; 2016) based on geophysical and paleoseismological investigations. An additional study (Del Gaudio et al., 2016) is

10   modelling ground motion in the Upper Rhine Graben with the help of the empirical green function approach (Del Gaudio et al., 2015). It is hoped that these studies will provide new insights for reducing epistemic uncertainty in fault-based PSHA of the Upper Rhine Graben.

Acknowledgments

The work presented in this paper was prepared for a master thesis project which was jointly funded by IRSN and ANR-11-

15   RSNR-0022 SINAPS@ project.

References

Baize, S., Cushing, E.M., Lemeille, F., and Jomard, H.: Updated seismotectonic zoning scheme of Metropolitan France, with reference to geologic and seismotectonic dataBulletin de la Societe Geologique de France, 184 (3), 225-259, doi: 10.2113/gssgfbull.184.3.225, 2013.

20   Baize, S., Reicherter, K., Thomas, J., Chartier, T., and Cushing, E. M.: Towards a Fault-based SHA in the Southern Upper Rhine Graben. In EGU General Assembly Conference Abstracts (Vol. 18, p. 14458), 2016.

Boore, D. M. and Atkinson, G. M.: Ground-motion prediction equations for the average horizontal component of PGA, PGV, and 5%-damped PSA at spectral periods between 0.01 s and 10.0 s. Earthquake Spectra, 24(1), 99-138. doi:10.1193/1.2830434, 2008.

25   Brun, J.P., Gutscher, M.-A., dekorp-ecors teams: Deep crustal structure of the Rhine Graben from dekorp-ecors seismic reflection data: A summary, Tectonophysics, 208 (1-3), pp. 139-147, doi: 10.1016/0040-1951(92)90340-C, 1992.

Campbell, K. W. and Bozorgnia, Y.: NGA ground motion model for the geometric mean horizontal component of PGA, PGV, PGD and 5% damped linear elastic response spectra for periods ranging from 0.01 to 10 s. Earthquake Spectra, 24(1), 139-171. doi: 10.1193/1.2857546, 2008.

Cauzzi, C. and Faccioli, E.: Broadband (0.05 to 20 s) prediction of displacement response spectra based on worldwide digital records. Journal of Seismology, 12(4), 453-475. DOI: 10.1007/s10950-008-9098-y, 2008.

Cornell, C. A.: Engineering seismic risk analysis. Bulletin of the Seismological Society of America, 58(5), 1583-1606, 1968.

Del Gaudio, S., Causse, M., and Festa, G.: Broad-band strong motion simulations coupling k-square kinematic source models with empirical Green's functions: the 2009 L'Aquila earthquake. Geophysical Journal International, 203(1), 720-736. doi : https://doi.org/10.1093/gji/ggv325, 2015.

Del Gaudio, S., Hok, S., Causse, M., Festa, G., and Lancieri, M.: Near fault broadband ground motion simulation with empirical Green's functions: the Upper Rhine Graben case study, EGU General Assembly 2016, held 17-22 April, 2016 in Vienna Austria, p.15403, 2016.

Edel, J. B., Whitechurch, H., and Diraison, M.: Seismicity wedge beneath the Upper Rhine Graben due to backwards Alpine push?. Tectonophysics, 428(1), 49-64. doi: 10.1016/j.tecto.2006.08.009, 2006.

Führmann, T., Heck, B., Knöpfler, A., Masson, F., Mayer, M., Ulrich, P.,Westerhaus, M., and Zippelt, K.: Recent surface displacements in the Upper Rhine Graben - Preliminary results from geodetic networks,Tectonophysics, 602, pp. 300-315, doi: 10.1016/j.tecto.2012.10.012, 2013.

Führmann, T., Westerhaus, M., Zippelt, K., and Heck, B.: Vertical displacement rates in the Upper Rhine Graben area derived from precise leveling. Journal of Geodesy, 88(8), 773-787, doi: 10.1007/s00190-014-0721-0, 2014.

Gutenberg, B., and Richter, C. F.: Seismicity of the Earth (Princeton Univ. Press), 310, 1954.

Hanks, T. C., and H. Kanamori: A moment magnitude scale, d. Geophys. Res., 84, 2348-2350, 1979.

IAEA SAFETY STANDARDS SERIES No. SSG-9 : Seismic hazards in site evaluation for nuclear installations, 56pp., 2010

Jomard, H., Cushing, E.M., Palumbo, L., Baize, S., David, C., and Chartier, T.: Transposing an active fault database into a seismic hazard fault model for nuclear facilities. Part A: Building a database of potentially active faults (BDFA) for metropolitan France, submitted in this issue.

LDG: Data file of French earthquakes from 1962 and on. Laboratoire de Détection et de Géophysique, Bruyères-le-Châtel, France, 2011.

McGuire, R. K.: FORTRAN computer program for seismic risk analysis (No. 76-67). US Geological Survey, 1976.

Nivière, B., Bruestle, A., Bertrand, G., Carretier, S., Behrmann J. and Gourry J.C.: Active tectonics of the southeastern Upper Rhine Graben, Freiburg area (Germany). Quaternary Science Reviews 27, 541-555. doi: 10.1016/j.quascirev.2007.11.018,2008.

Ordaz, M., Martinelli, F., Aguilar, A., Arboleda, J., Meleti, C., and d'Amico, V.: CRISIS 2014. Program for computing seismic hazard. Instituto de Ingeniería. Universidad Nacional Autónoma de México., 2014.

Rotstein, Y., and Schaming, M.: The Upper Rhine Graben (URG) revisited: Miocene transtension and transpression account for the observed first-order structures. Tectonics 30, TC3007, doi: 10.1029/2010TC002767, 2011.

Schumacher, M.E.: Upper Rhine Graben: Role of preexisting structures during rift evolution, Tectonics, 21 (1), pp. 6-1-6-17, doi: 10.1029/2001TC900022, 2002.

Stucchi, M., Rovida, A., Capera, A. G., Alexandre, P., Camelbeeck, T., Demircioglu, M. B., Gasperini, P., Kouskouna, V., Musson, R. M. W., Radulian, M., Vilanova, S., Baumont, D., Bungum, H., Fäh, D., Lenhardt, W., Makropoulos, K., Martinez Solares, J. M., Scotti, O., Živčić, M., Albini, P., Batllo, J., Papaioannou, C., Tatevossian, R., Locati, M., Meletti, C., Viganò, D., Giardini, D., and Sesetyan, K.: The SHARE European earthquake catalogue (SHEEC) 1000–1899. Journal of

5 Seismology, 17(2), 523-544. doi: 10.1007/s10950-012-9335-2, 2013.

Wells, D. L. and Coppersmith, K. J.: New empirical relationships among magnitude, rupture length, rupture width, rupture area, and surface displacement. Bulletin of the seismological Society of America, 84(4), 974-1002, 1994.

Wesnousky, S. G.: Earthquakes, Quaternary faults, and seismic hazard in California. Journal of Geophysical Research: Solid Earth, 91(B12), 12587-12631, 1986.

10 Zhao, J. X., Zhang, J., Asano, A., Ohno, Y., Oouchi, T., Takahashi, T., Ogawa, H., Irikura, K., Thio H. K., Somerville, P. G., Fukushima, Y., and Fukushima, Y.: Attenuation relations of strong ground motion in Japan using site classification based on predominant period. Bulletin of the Seismological Society of America, 96(3), 898-913. doi: 10.1785/0120050122, 2006.

Fault Name	Length (km)	Maximum magnitude (WC94 normal fault coefficients)	Dip (°) Min	Max	Fault Slip Rate (mm/y) Min	Max
FR 1	36	6.5	60	80	0.04	0.1
FR 2	27	6.4	60	80	0.04	0.1
FR 3	20	6.3	60	80	0.04	0.1
FFN 1	15	6.2	60	80	0.05	0.15
FFN 2	50	6.7	60	80	0.05	0.15
FFN 3	35	6.3	60	80	0.05	0.15
FRO 1	36	6.5	40	60	0.01	0.05
FRO 2	16	6.2	40	60	0.01	0.05
FRO 3	27	6.3	40	60	0.01	0.05

15 **Table 1 : Example of fault parameters considered in the calculations (seismogenic depth of 15km, steepest dip of the faults). FR = Rhine River Fault; FFN = Black Forest Fault; FRO = West Rhenish Fault. (See Figure 4 of Part A)**

Fault Name	Annual rate of M≥6 for the GR-model (#N/year) Min slip rate	Max slip rate	Annual rate of the characteristic earthquake (#N/year) Min slip rate	Max slip rate
FR 1	1.35×10^{-4}	3.38×10^{-4}	1.08×10^{-4}	2.70×10^{-4}
FR 2	1.13×10^{-4}	2.83×10^{-4}	1.17×10^{-4}	2.92×10^{-4}
FR 3	8.70×10^{-5}	2.18×10^{-4}	1.14×10^{-4}	2.85×10^{-4}
FFN 1	9.30×10^{-5}	2.79×10^{-4}	1.53×10^{-4}	4.59×10^{-4}
FFN 2	2.02×10^{-4}	6.06×10^{-4}	9.90×10^{-5}	2.97×10^{-4}
FFN 3	2.00×10^{-4}	6.00×10^{-4}	2.64×10^{-4}	7.92×10^{-4}

FRO 1	4.50 x 10^{-5}	2.25 x 10^{-4}	2.70 x 10^{-5}	1.35 x 10^{-4}
FRO 2	1.80 x 10^{-5}	9.00 x 10^{-5}	3.06 x 10^{-5}	1.53 x 10^{-4}
FRO 3	3.50 x 10^{-5}	1.75 x 10^{-4}	2.85 x 10^{-5}	2.64 x 10^{-4}

Table 2 : Example of seismic activity for each fault deduced from their slip rate and geometries (Table 1, seismogenic depth of 15km, steepest dip of the faults) and μ=3 10^{10} N.m^{-2}. FR = Rhine River Fault, FFN = Black Forest Fault and FRO = West Rhenish Fault.

Identifier	References	Spectral period range (s)	Distance range (km)	Magnitude range	Distance metrics	Origin of data
BA08	Boore and Atkinson, 2008	0 - 10	1 - 200	5 - 8	R$_{JB}$	California, Taiwan
CB08	Campbell and Bozorgnia, 2008	0 - 10	0 - 200	4 - 8.5	R$_{Rup}$	California, Taiwan
CF08	Cauzi and Faccioli, 2008	0.01 - 20	6 - 150	5 - 7.2	R$_{Focal}$	World crustal regions
ZH06	Zhao et al., 2006	0 - 5	0.4 - 300	5 - 8.4	R$_{Rup}$	Japan Crustal regions

5   **Table 3 : GMPEs considered in this study**
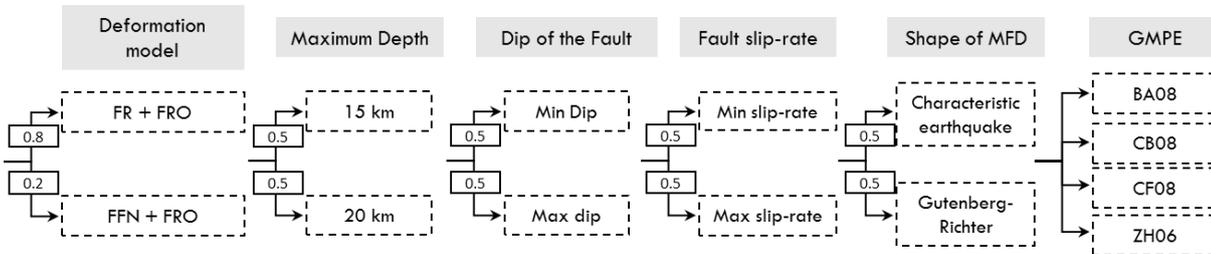
Figure 1 : Logic tree explored in this study: The weight attributed to each hypothesis is shown by the number in the boxes. (GMPEs) are explored separately (no weight attributed).
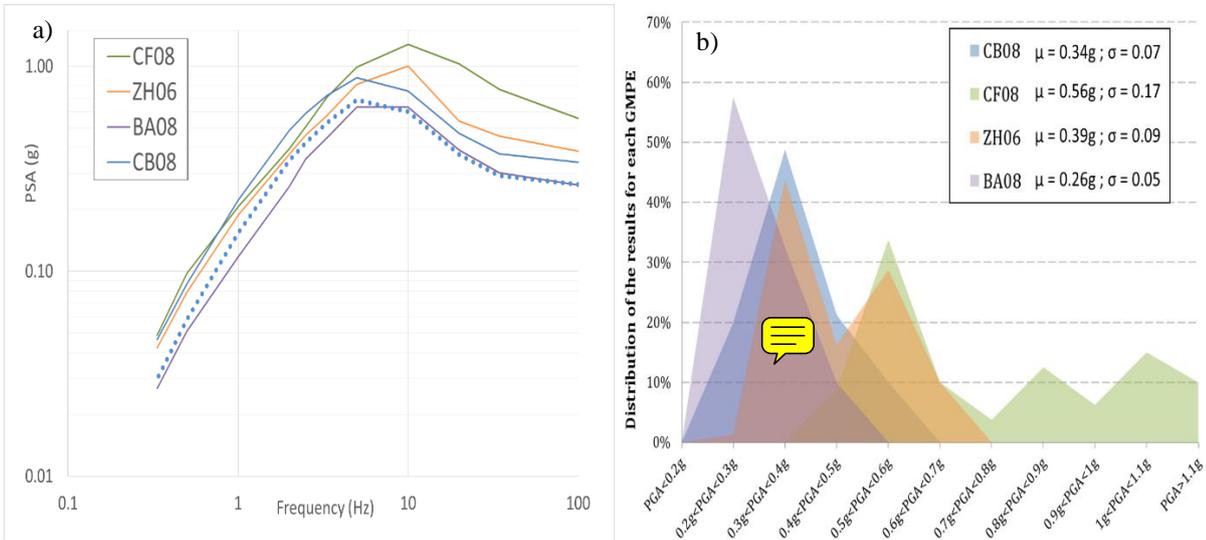
Figure 2 : Left: Uniform Hazard Spectra for a return period of 10,000 years. Mean UHS of the logic tree in black. Mean UHS for each GMPE in color. The dotted line is the branch used for the sensitivity analysis. Right: dispersion of PGA at 10,000 for each GMPE branch resulting from the exploration of epistemic uncertainties shown in Figure 1.
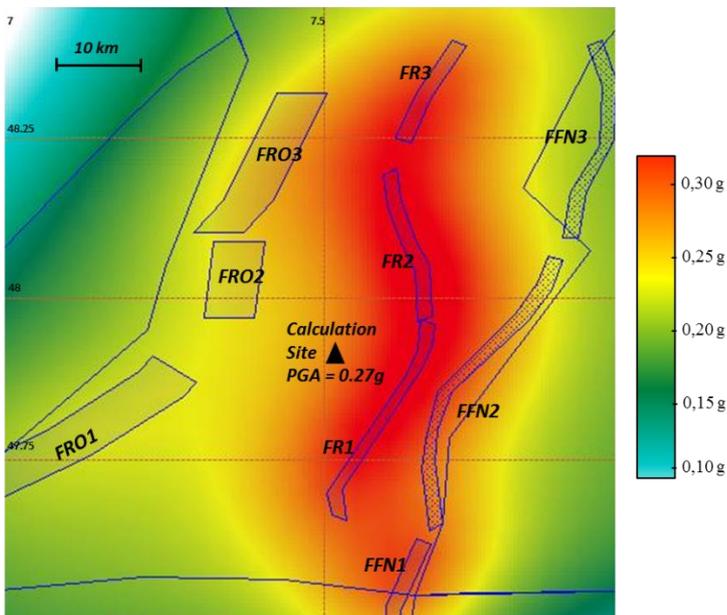
Figure 3 : PGA seismic hazard map at a return period of 10,000 years for the reference logic tree branch: Rhine River Fault active, seismogenic depth at 15km, steepest dip for the faults, low slip rate values for the faults, Gutenberg-Richter MFD and the CB08 GMPE. Polygons represent the fault projections at the surface of the modeled faults (hachured polygons indicate the faults
10 **sources that are considered inactive in this calculation). Contours of the background area-source are shown as well. Figure produced with the CRISIS software. FR = Rhine River Fault, FFN = Black Forest Fault and FRO = West Rhenish Fault.**
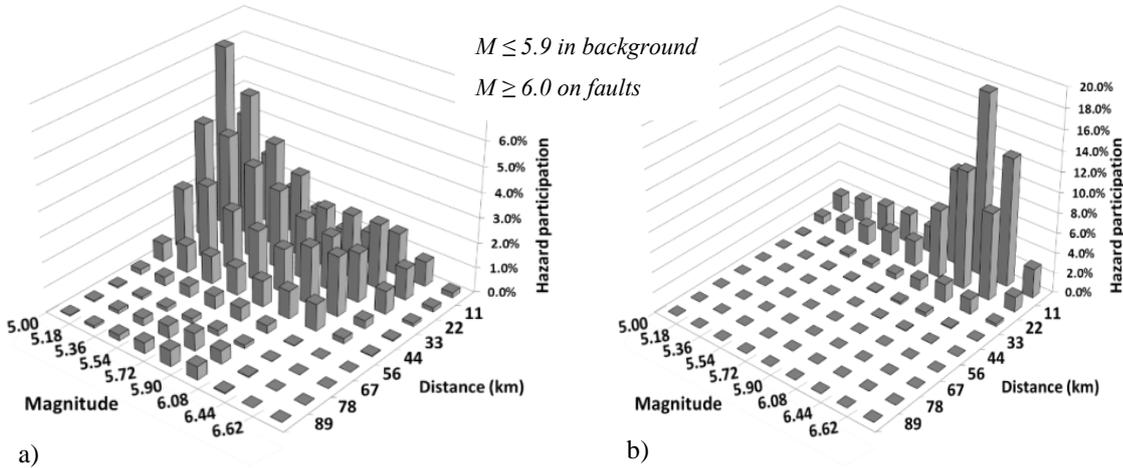
Figure 4 : Seismic hazard disaggregation for PGA at return periods of 475 on the left (PGA = 0.06 g) and 10,000 years on the right (PGA = 0.27 g). Branch of the logic tree: Rhine River Fault active, seismogenic depth of 15km, steepest dip of the faults, slowest slip rate, Gutenberg-Richter frequency-magnitude distribution and CB08.
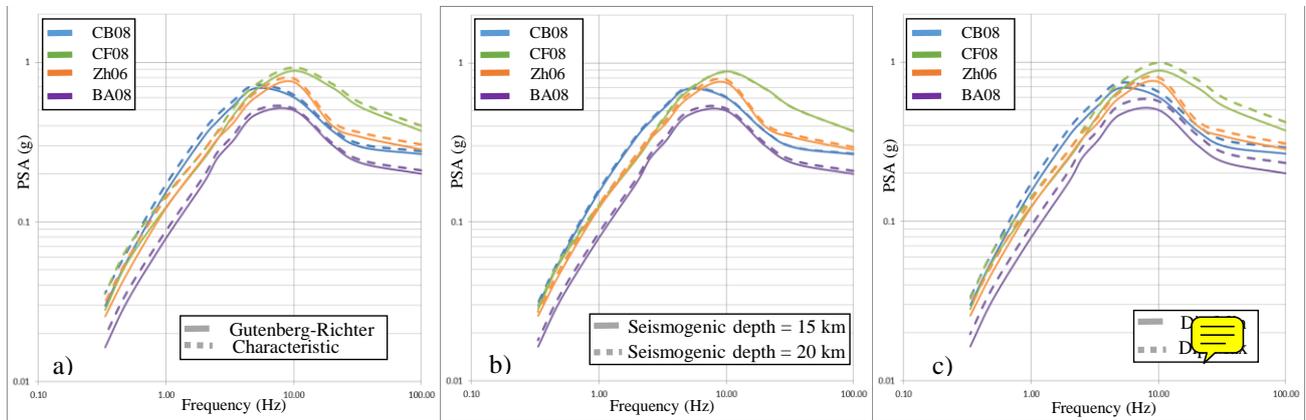
Figure 5 : Impact of the different uncertainties explored in the logic tree on the UHS at 10,000 years for the site of interest. From left to right: Shape of the MFD, Seismologic depth and Dip of the faults.
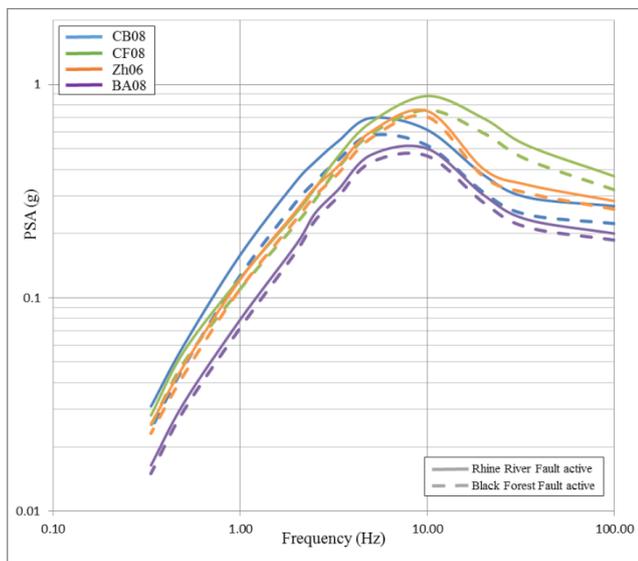
Figure 6: UHS at 10,000 years return period considering four GMPEs : CB08, CF08, ZH06 and BA08 (see Table 3 for references). Seismogenic depth of 15km, the steepest dip of faults, the slowest slip rate, a Gutenberg-Richter frequency-magnitude distribution, the seismic moment method and μ=3 10^{10} N.m^{-2}.
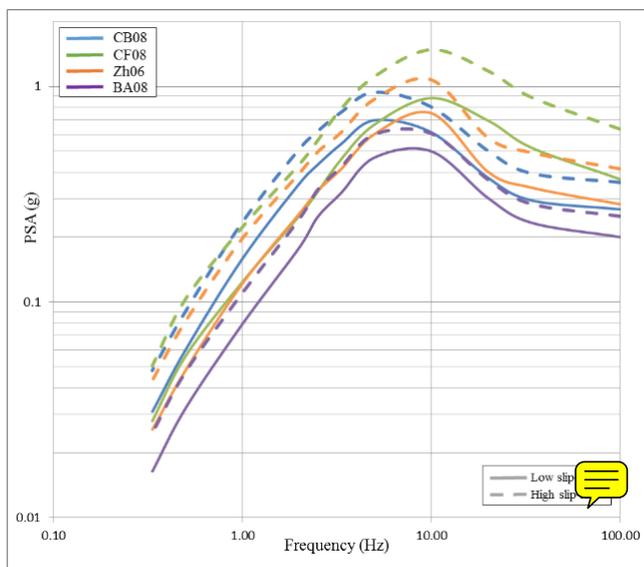
Figure 7: Comparison of UHS based on the Rhine River Fault geodynamic model considering two slip rate values. Seismogenic depth of 15 km, steepest dip of faults, a Gutenberg-Richter frequency-magnitude distribution, the seismic moment method and μ=3 10^{10} N.m^{-2}.

Annex

Fault_Name	Segment_Name	Segment name PSHA	Dip (°)	± Dip	Dip PSHA	Depth (km)	± Depth	Depth PSHA	Length (km)	Length PSHA	Neotectonic_Age	slip rate (mm/yr)	Slip rate PSHA	Robustness (IR)	Bibliography for BDFA
Rhine River Fault	FRR-1	FR1	65	15	70 ± 10	15	5	15 to 20	35	36	Quaternary	UnDef	0,04 to 0,1	15.4	Segmentation & geometry (Rotstein et al., 2005 ; Nivière et al., 2008 ; Behrmann, 2003) - Slip rate (Nivière et al., 2008)
	FRR-2	FR2	65	15	70 ± 10	15	5	15 to 20	25	27	Quaternary	0,04 - 0,09	0,04 to 0,1	11	
	FRR-3	FR3	70	99	70 ± 10	15	5	15 to 20	20	20	Undetermined	< 0,1	0,04 to 0,1	4.4	
West Rhenish Fault	Belfort-Guebwiller	FRO1	50	99	50 ± 10	3.5	99	15 to 20	36	36	Pliocene	UnDef	0,01 to 0,05	14.3	Segmentation & geometry (Rotstein et Schaming., 2008, Ford et al., 2007, Bertrand, 2005) - Slip rate (Nivière et al., 2008 ; Cornu et Bertrand 2005)
	Guebwiller-Colmar	FRO2	55	99	50 ± 10	2.5	99	15 to 20	16	16	Pliocene	UnDef	0,01 to 0,05	6.6	
	Colmar-Sélestat	FRO3	60	99	50 ± 10	1.5	99	15 to 20	27	27	Pliocene	UnDef	0,01 to 0,05	6.6	
Black Forest Fault	FFN-1	FFN1	40	99	70 ± 10	15	5	15 to 20	20	15	Quaternary	UnDef	0,05 to 0,15	11	Segmentation & geometry (Behrmann et al., 2003 ; Nivière et al., 2008) - Slip rate (Nivière et al., 2008)
	FFN-2	FFN2	50	99	70 ± 10	15	5	15 to 20	50	50	Quaternary	0,07 - 0,18	0,05 to 0,15	11	
	FFN-3	FFN3	40	99	70 ± 10	15	5	15 to 20	35	35	Miocene	UnDef	0,05 to 0,15	8.8	

Figure Annex: a) Potentially active faults from BDFA (in black), selected segments for PSHA calculation in colour (depending on the age of the last movement on the fault). b) Fault model as produced for PSHA. Black lines correspond to the surficial trace of the faults, in light blue the projection of fault planes at the surface (taking into account a 15km depth and the max. dip angle), in light red the closest fault to FSH (Fessenheim NPP). c) Table containing principal parameters as exported from BDFA (grey and white columns) table and their transposition into the parametric PSHA fault model (light green columns).